Pharmaceutical Sciences and Drug Design
ISSN: 3062-4428
2025, Volume 5, Issue 2, Page No: 220-242

Available online at: www.galaxypub.co/page/journals

Galaxy Publication

Mechanistic Insights into Zuojin Pill in Chronic Atrophic Gastritis: Modulation of PI3K/Akt-Mediated Apoptosis and Gastric Mucosal Barrier Integrity

Hiroshi Nakamura[1]*, Yuta Kato[1]

[1]Department of Pharmaceutical Sciences and Molecular Design, Faculty of Pharmacy, Nagoya University, Nagoya, Japan.

***E-mail** ✉ hiroshi.nakamura@outlook.com

Received: 17 August 2026; **Revised:** 26 October 2026; **Accepted:** 03 November 2026

ABSTRACT

In clinical practice, the Zuojin Pill (ZJP) is commonly used to manage chronic atrophic gastritis (CAG) and effectively alleviates symptoms such as emesis, discomfort, and abdominal bloating. Yet, the mechanistic basis for ZJP's therapeutic action in CAG remains unclear. The objective of this work was to define the distinctive role of ZJP in CAG management along with its potential mode of action. An experimental CAG model was generated through alternating exposure to ammonia solution and sodium deoxycholate, together with erratic dietary intake. Evaluations were conducted on ZJP's impact on body mass, serum biochemical parameters, and overall physiological status. Assessment of mucosal lesions and gastric mucosal depth was performed via HE staining and AB-PAS staining. Furthermore, network pharmacology, coupled with molecular docking, enabled the prediction of regulatory pathways and key bioactive constituents of ZJP relevant to CAG therapy. Quantification of molecules linked to apoptosis, gastric mucosal barrier integrity, and the PI3K/Akt signaling cascade was carried out using RT-PCR, immunohistochemistry, immunofluorescence, and Western blotting. Findings revealed that ZJP substantially improved overall physiological condition in CAG rats, attenuated body mass loss and gastric tissue pathology, and reduced serum biochemical markers. Network pharmacology and molecular docking analyses identified that ZJP targets CAG by suppressing inflammation, inhibiting apoptosis, and preserving the gastric mucosal barrier via the PI3K/Akt signaling pathway. Subsequent experimental validation confirmed that ZJP visibly regulated the levels of critical proteins governing gastric mucosal cell apoptosis, namely Bax, Bad, Apaf-1, cleaved caspase-3, cleaved caspase-9, cytochrome c, Bcl-2, and Bcl-xl. Additionally, ZJP markedly restored the protein abundance of Occludin, ZO-1, Claudin-4, and E-cadherin. This investigation demonstrated that ZJP exerts therapeutic effects on CAG by suppressing the PI3K/Akt signaling pathway, providing a scientific rationale for its appropriate clinical use.

Keywords: Zuojin pill, Chronic atrophic gastritis, Network pharmacology, Molecular docking, PI3K/Akt signaling pathway

How to Cite This Article: Nakamura H, Kato Y. Mechanistic Insights into Zuojin Pill in Chronic Atrophic Gastritis: Modulation of PI3K/Akt-Mediated Apoptosis and Gastric Mucosal Barrier Integrity. Pharm Sci Drug Des. 2025;5(2):220-42. https://doi.org/10.51847/fEFfm72Jfa

Introduction

Chronic atrophic gastritis (CAG) constitutes a gastric condition hallmarked pathologically by decreased gastric acid production, thinning of the gastric mucosa, and intestinal metaplasia [1, 2]. Recognized as a pivotal precancerous state for gastric carcinoma—the third leading contributor to cancer mortality worldwide according to 2018 statistics [3]—CAG has been ascribed in prior research to a multifactorial etiology involving *Helicobacter pylori* colonization, defective immune control, and aberrant energy homeostasis, with its disease mechanisms tied to oxidative injury, inflammatory responses, and endothelial, along with mucosal dysfunction [4, 5]. Contemporary therapeutic strategies for CAG hinge chiefly on gastroprotective agents, symptom-relieving medications, vitamin C supplementation, and proton pump inhibitors; however, their extended treatment

timelines, invasive nature, and unfavorable side-effect profiles restrict their practical use [6, 7]. As such, an acute need persists for adjunctive and alternative remedies targeting CAG.

Traditional Chinese medicine (TCM) has distinct advantages in CAG management due to its dual healing and modulatory properties, broad applicability, and low incidence of adverse reactions [8-11]. The time-honored Chinese remedy Zuojin Pill (ZJP), chronicled in the Yuan-era text Danxi prescription therapy, constitutes a celebrated TCM formulation deployed clinically against CAG and comprises two botanical ingredients: Coptidis Rhizoma and Euodiae Fructus [12]. Modern pharmacological investigations have documented that ZJP possesses diverse attributes, including reduced inflammation [12], bacterial suppression [13], apoptosis mitigation [14], and mucosal protection [15], demonstrating a significant therapeutic impact on gastrointestinal ailments. One recent report indicated that ZJP operates as an inflammation blocker to rectify systemic metabolic imbalances in patients, representing a crucial facet of its action in chronic gastritis [16]. Still, the comprehensive mechanism by which ZJP counteracts chronic atrophic gastritis remains to be fully elucidated, underscoring the need for deeper inquiry into its underlying therapeutic mechanisms.

Propelled by rapid advances in bioinformatics, network pharmacology has emerged as an innovative discipline that applies mathematical and computational frameworks to map the multifaceted relationships between botanical formulas and pathological conditions [17]. This approach introduces fresh perspectives for pharmaceutical inquiry, particularly for TCM explorations rooted in complex systems. An expanding body of research confirms that network pharmacology can unravel the prospective mechanistic underpinnings of multi-component, multi-target therapeutics by dissecting elaborate, hierarchical interaction networks [18, 19]. Molecular docking is a routine technique for probing binding interfaces between small ligands and macromolecular targets. The present study endeavors to delineate the signature effects of ZJP on histopathological restoration of gastric tissue in CAG by integrating empirical methods, thereby providing experimental validation for its judicious clinical application. Leveraging high-throughput analytical modalities such as network pharmacology and molecular docking, the research further aims to uncover the molecular and biological underpinnings of ZJP's anti-CAG action, along with its putative active entities, providing data-driven foundations for future, innovative drug development targeting CAG intervention **(Figure 1)**.

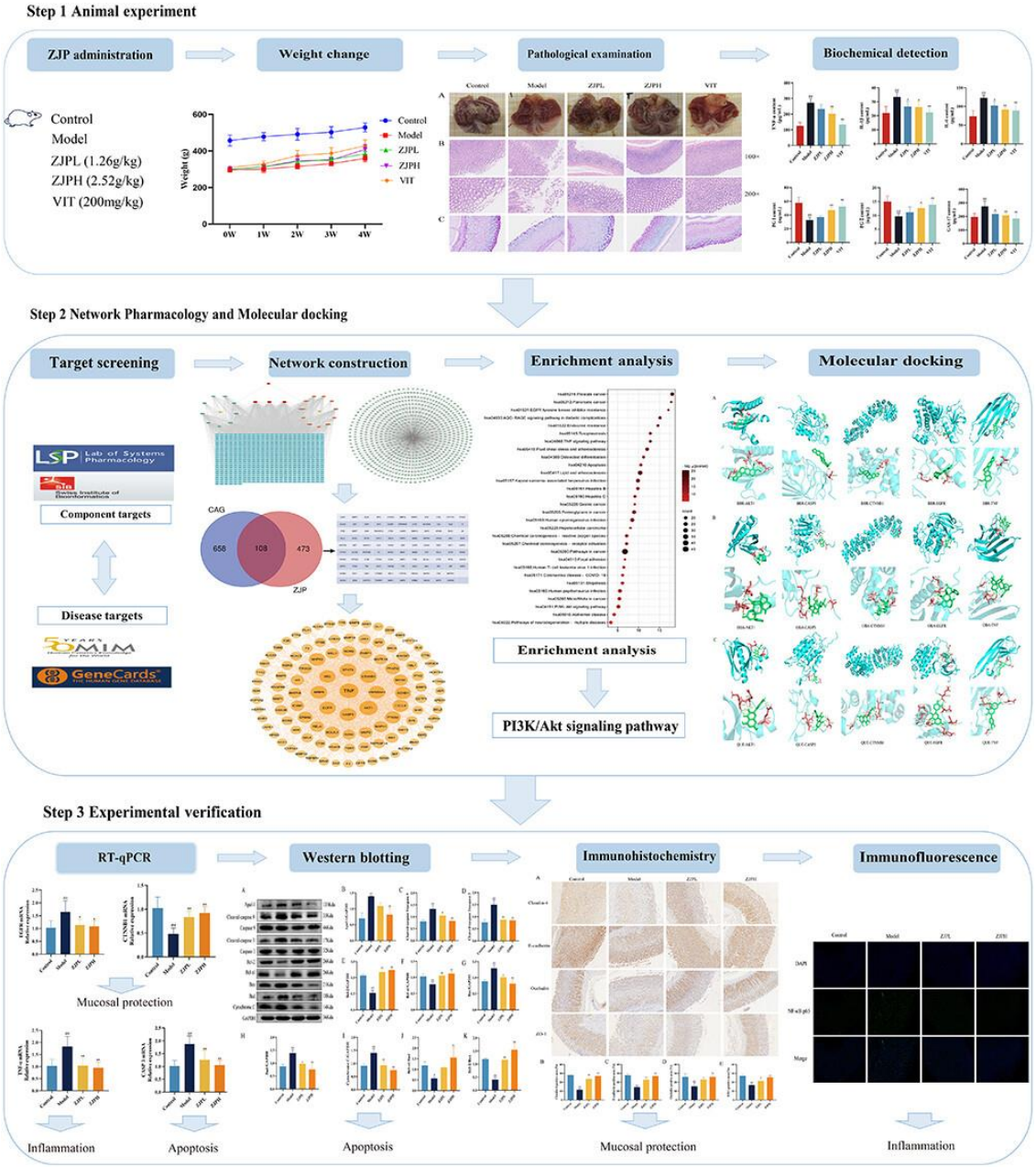

Figure 1. Flow chart of this study. Abbreviations: ZJPL = Zuojin Pill low dose (1.26g/kg); ZJPH = Zuojin Pill high dose (2.52g/kg); VIT = Vitacoenzyme (200 mg/kg). #P < 0.05 and ##P < 0.01 vs control group. P < 0.05 and P < 0.01 vs model group.

Materials and Methods

Reagents

The herbal materials Coptidis Rhizoma (Lot: 21030801) and Euodiae Fructus (Lot: 21101401) were procured from Beijing LVYE Pharmaceutical Co., Ltd. (Beijing, China). Supplies of sodium deoxycholate (Lot: CD33141310) came from Beijing Zhongke Ruijin Technology Co., Ltd., and ammonia (Lot: 2023AS0328) was provided by Biotechnology Co., Ltd. Vitacoenzyme tablets (Lot No. 221002) originated from Guangxi Dahai Sunshine Pharmaceutical Co., Ltd. All antibodies and associated reagents were purchased through commercial channels.

Preparation of ZJP

A mixture of Coptidis Rhizoma and Euodiae Fructus at a 6:1 weight ratio was steeped in purified water for 30 min. Two successive rounds of thermal extraction were then carried out, each lasting 1 h. All filtrates were

combined and processed by rotary evaporation, then concentrated and dried to yield a powdered extract, which was stored at 4 °C under refrigeration [20]. The resulting dry powder accounted for 18.75% of the original herb weight.

Animals and experimental design

Male Sprague-Dawley rats (180–200g) of specific pathogen-free (SPF) status were acquired from Sibeifu Biotechnology Co., Ltd. (Beijing, China, license No.: SCXK (Beijing) 2019–0010). Housing conditions consisted of ventilated polypropylene cages maintained at ambient room settings (temperature: 25 ± 0.5 °C, humidity: 55% ± 5%, with a 12 h light/12 h dark cycle), and both drinking water and standard chow were available without restriction. All experimental procedures involving animals complied with the Laboratory Care and Use Guidelines. Ethical clearance was granted by the Ethics Committee of the Chinese PLA General Hospital (Approval ID: IACUC-2021-0022).

Upon completion of a one-week adaptation and quarantine interval, a total of 34 SD rats were randomly assigned into two groups: 8 animals constituted the control group. At the same time, the remaining 26 were placed in the model group. Induction of CAG followed an established methodology [21]. In essence, the model group animals received alternating administrations of 0.1% ammonia solution and 20 mmol/L sodium deoxycholate solution, coupled with an irregular feeding and fasting regimen. After 10 weeks, 2 rats from each cohort (control and model) were randomly selected to confirm successful CAG induction. Subsequently, the CAG-afflicted rats were allocated into four treatment arms: a model group, a positive drug group administered Vitacoenzyme (VIT, 200 mg/kg), a ZJP low dose group (ZJPL, 1.26g/kg), and a ZJP high dose group (ZJPH, 2.52g/kg) [22]. Drug delivery was performed once daily via oral gavage for a continuous 4-week treatment phase **(Figure 2).**

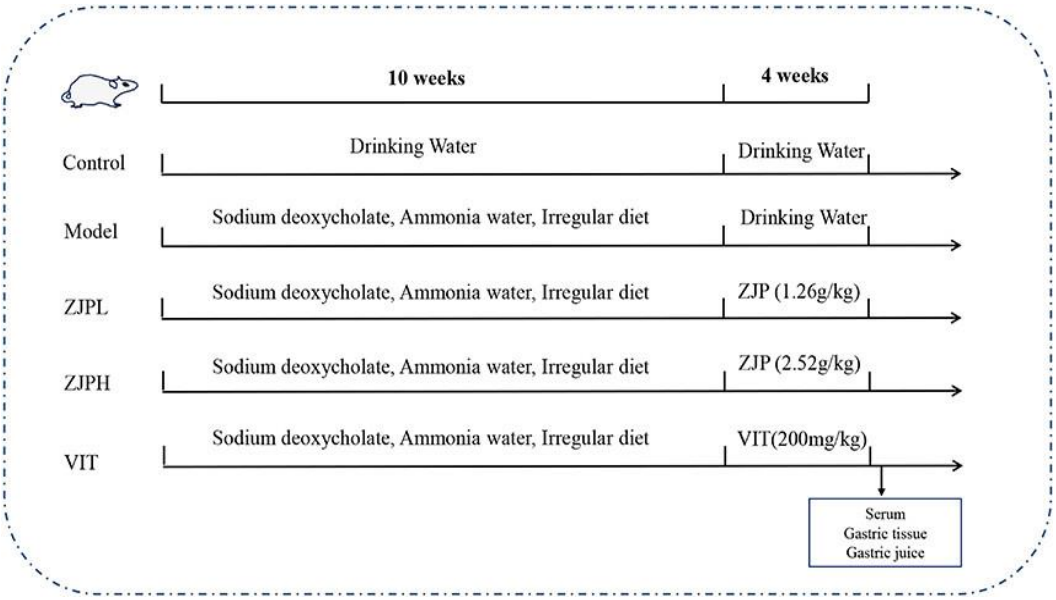

Figure 2. The schematic overview of the experimental design. Abbreviations: ZJPL = Zuojin Pill low dose (1.26g/kg); ZJPH = Zuojin Pill high dose (2.52g/kg); ZJP = Zuojin Pill; VIT = Vitacoenzyme (200 mg/kg).

Sample collection

When the experimental period concluded, food was withheld from all rats for 24 h while they retained free access to water. Euthanasia was first performed using a 20% ethyl carbamate solution. Blood was then drawn from the abdominal aorta, and the gastric tissues were harvested. Serum was separated via centrifugation and kept at −80 °C until further testing. Each gastric specimen was bisected: one portion was placed in 10% paraformaldehyde for later pathological evaluation, and the counterpart was frozen at −80 °C for upcoming molecular analyses. To conclude the collection, gastric juice was collected and spun at 4 °C and 13,000 rpm for 10 min. The clear supernatant was isolated, and the pH was measured.

Pathological observation

Gastric specimens were preserved by immersion in 10% neutral formalin solution, then dehydrated in graded ethanol and xylene. After dehydration, the tissues were infiltrated with and embedded in paraffin wax. Consecutive sections sliced at a thickness of 4 μm were produced and stained using hematoxylin and eosin (H&E) as well as Alcian blue-Periodic acid-Schiff (AB-PAS) techniques. Visualization and assessment of gastric mucosal histopathology were conducted under a Nikon microscope (Nikon Instruments, Japan).

Biochemical detection

Circulating concentrations of interleukin-6 (IL-6), interleukin-1β (IL-1β), and tumor necrosis factor-α (TNF-α) in serum were quantified in strict accordance with the manufacturer's guidelines. In addition, commercially available ELISA kits were applied to determine the levels of Pepsinogen I (PG I), Pepsinogen II (PG II), and Gastrin17 (GAS-17).

TdT-mediated dUTP nick-end labeling (TUNEL) staining

Initially, gastric tissue was fixed in paraformaldehyde, embedded in paraffin, and sectioned at 4 μm. The proportion of cells undergoing programmed cell death was then quantified through TUNEL staining, following a previously outlined protocol [5]. Apoptotic cells were visualized by light microscopy, and results were reported as the mean count of TUNEL-positive cells per microscopic field at 200× magnification.

Measurement of gastric pH

Once centrifugation was complete, the pH of gastric juice from every group was assessed using high-accuracy pH indicator paper [23]. To maintain consistency in the qualitative readout, the same operator read the pH value immediately against a colorimetric reference card.

Data preparation of network pharmacology

Selection of target compounds for ZJP

The chemical ingredients of ZJP were harvested from the Traditional Chinese Medicine Systems Pharmacology Database (TCMSP, http://lsp.nwu.edu.cn/tcmsp.php). Screening of promising compounds applied dual filters: an oral bioavailability (OB) score of 30% or above and a drug-likeness (DL) value no lower than 0.18. Next, the molecular targets associated with these qualifying constituents were mined from the SwissTargetPrediction database (http://www.swisstargetprediction.ch/), requiring a probability greater than 0. Finally, a graphical "ZJP-compounds-targets" network was constructed using Cytoscape 3.8.0 software (Cytoscape Consortium, National Institute of General Medical Sciences, USA).

Identification of CAG targets

Putative targets linked to CAG were sourced from both GeneCards (http://www.genecards.org/) and Online Mendelian Inheritance in Man (OMIM, http://www.omim.org/), using the terms "chronic atrophic gastritis" or "CAG." After pooling records from these two databases, duplicate entries were purged, and the consolidated, standardized collection of targets formed the CAG disease target dataset. The subsequent "CAG-target" interaction map was generated using Cytoscape 3.8.0.

Construction of protein-protein interaction (PPI) network

An overlap analysis between the CAG-linked targets and ZJP-associated targets was performed and displayed in a Venn diagram generated via an online Venn tool (https://bioinformatics.psb.ugent.be/webtools/Venn/), from which shared targets were extracted. The PPI network was then assembled in the String platform (https://www.string-db.org/) and visualized using Cytoscape 3.8.0.

GO and KEGG pathway enrichment analysis

Functional characterization, including Kyoto Encyclopedia of Genes and Genomes (KEGG) pathway mapping and Gene Ontology (GO) categorization, was conducted by submitting the overlapping targets to the Database for Annotation, Visualization and Integrated Discovery (DAVID; https://david.ncifcrf.gov/). A threshold of $P < 0.05$ defined statistically enriched GO terms and KEGG pathways. For purposes of graphical representation, the 20 most significant KEGG pathways were selected, along with the top 10 enriched terms from each GO domain—cellular component, biological process, and molecular function.

Total RNA extraction and real-time PCR

Whole RNA was extracted from gastric tissue homogenates using a dedicated RNA extraction kit (Huaxingbio, Beijing, China), after which messenger RNA was reverse transcribed into cDNA to serve as the template for amplification. RT-qPCR was performed with SYBR Green PCR Master Mix (Huaxingbio, Beijing, China) on the 7500 Fast Real-Time PCR System (Applied Biosystems, Foster City, CA, USA). Relative quantification was performed using the $2^{-\Delta\Delta CT}$ formula, with GAPDH as the internal reference gene.

Western blotting assay

Gastric tissue specimens were processed for total protein isolation using an ice-cold radioimmunoprecipitation assay (RIPA) lysis buffer that had been freshly supplemented with phenylmethylsulfonyl fluoride (PMSF) and a phosphatase inhibitor blend. A BCA Protein Assay Kit facilitated the measurement of protein concentrations across all samples. Equal protein aliquots were fractionated via sodium dodecyl sulfate-polyacrylamide gel electrophoresis (SDS-PAGE) before being transferred electrophoretically onto polyvinylidene difluoride (PVDF) sheets. A 2-hour blocking step was then carried out at room temperature. Overnight probing at 4 °C followed, using a panel of primary antibodies. The following morning, membranes were washed 5 times in TBS containing 0.1% Tween 20 (TBST), then incubated for 2 hours at room temperature with the matching secondary antibody. Five additional TBST rinses were performed before signal development using an ECL Plus chemiluminescence kit. GAPDH functioned as the endogenous normalization control. Band intensities from the captured digital images were analyzed densitometrically using ImageJ (National Institutes of Health, Bethesda, United States).

Immunohistochemistry

Fixed gastric tissue biopsies were first immersed in 10% formaldehyde, then embedded in paraffin and sectioned. Mounted sections were dewaxed and rehydrated via descending ethanol concentrations. For epitope unmasking, slides were heated in citric acid-based antigen retrieval buffer (pH 6.0) within a microwave oven for a total of 16 min. After benchtop cooling, three sequential 5-minute immersions in phosphate-buffered saline (PBS) at pH 7.4 were carried out. Endogenous peroxidase activity was extinguished by applying 3% hydrogen peroxide to the sections in the dark for 25 min at room temperature, after which a 30-minute blocking procedure with 3% bovine serum albumin was deployed to saturate non-specific binding sites. The tissues were subsequently left overnight at 4 °C under one of the following rabbit-derived primary antibodies: anti-ZO-1 polyclonal (Huaxingbio, HX19906, 1:100), anti-Claudin-4 polyclonal (Huaxingbio, HX13369, 1:100), anti-E-cadherin polyclonal (Huaxingbio, HX14050, 1:300), or anti-Occludin polyclonal (Huaxingbio, HX20200, 1:300). The next stage involved applying an HRP-linked goat anti-rabbit secondary antibody (Huaxingbio, HX2031, 1:5000), followed by hematoxylin counterstaining. For each slide, three arbitrarily chosen microscopic fields were photographed. Protein abundance was quantified as integrated optical density (IOD), calculated in ImageJ (National Institutes of Health, Bethesda, United States).

Immunofluorescence

Sections cut from paraffin-embedded gastric material underwent dewaxing and solvent exchange through a graded ethanol lineup, then were subjected to antigen retrieval by heating in ethylenediaminetetraacetic acid (EDTA) buffer. Triple rinses in phosphate-buffered saline (PBS) were performed, and the sections were incubated in 1% BSA for 30 minutes at ambient temperature to reduce non-specific antibody binding. A 4 °C overnight incubation with anti-NF-κB p65 antibody was performed. The following day, sections were incubated with the corresponding secondary antibody for 1 h at room temperature, nuclear DNA was labeled with 4,6-diamino-2-phenylindole (DAPI), and fluorescent images were acquired on a confocal microscope (NIKON Eclipse C1, Nikon Instruments Inc., Japan). Image capture and processing were handled by a NIKON DS-U3 (Nikon Instruments Inc., Japan) for quantitative readout of NF-κB p65 immunofluorescence signal. Integrated optical density (IOD) values were extracted using ImageJ.

Molecular docking

Following the prioritization of hub targets and principal bioactive components from both the PPI network and the "key ingredients-targets" interaction map for ZJP's action in CAG, in silico docking was carried out. Crystallographic structures corresponding to the chosen core targets were downloaded from the RCSB database

(https://www.rcsb.org/), and the mol2 structural files for the major ingredients were sourced from the TCMSP database. Docking calculations were performed with AutoDock Tools 1.5.6, and the resulting binding modes were graphically depicted in PyMol.

Statistical analysis

The computational analysis of study data relied on SPSS 26.0 (International Business Machines Corporation, New York, United States). Every dataset is presented as the arithmetic mean ± standard deviation (SD). Intergroup statistical comparisons employed either a two-tailed Student's t-test or one-way analysis of variance (ANOVA) as dictated by the experimental design. Visual plots of the findings were generated in GraphPad Prism (version 8.0). Throughout the investigation, P values below 0.05 were considered statistically significant.

Results and Discussion

Evaluation of CAG model establishment

A verification step was performed after the 10-week continuous induction protocol to determine whether the modeling procedure was effective. Assessments of the model group animals revealed a deceleration in weight gain, along with signs of apathy, reduced locomotor activity, coat dishevelment, and a dull hair sheen. Inspection of the gastric mucosa in these rats revealed thinning of the tissue, diminishment and flattening of the mucosal ridges, and a perceptible loss of tissue pliability **(Figure 3a)**. Examination of HE-stained sections revealed the disappearance of native glandular structures, focal detachment of the mucosal layer, and neutrophil trafficking into the mucosa in the model animals **(Figure 3b)**. Body weight measurements taken after the modeling period showed a pronounced drop compared with the control cohort **(Figure 3c).**

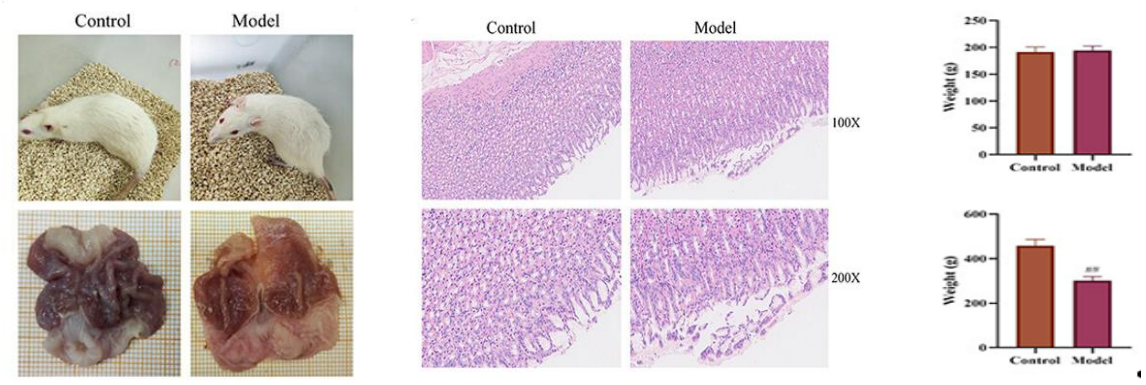

a) b) c

Figure 3. Evaluation of the CAG model establishment: (a) General state of rats and macroscopic manifestation of gastric tissue in the control and model groups, (b) HE staining of gastric tissue in the control group and model group, and (c) Changes in body weight of rats in the control group and model group. All data were expressed as means ± standard deviation (SD). An unpaired two-tailed Student's t-test analyzed two group comparisons. ##P < 0.01 vs control group.

Effect of ZJP on general condition and body weight in CAG rats

Progressive body mass decline is the most characteristic indicator of CAG. Throughout the modeling timeline, mean body weights within the model group lagged considerably behind those of the control animals. The cohorts receiving ZJP and vitacoenzyme both demonstrated appreciable weight gain, suggesting equivalent therapeutic efficacy in the CAG rat model **(Figure 4a)**. Analysis of gastric juice revealed that pH readings in the model arm were substantially elevated over those of the control arm. ZJP exerted a robust regulatory effect, restoring gastric pH toward normal levels **(Figure 4b).**

Additionally, control rats sustained an excellent overall presentation—their coats remained glossy and their movements unrestricted. In contrast, model rats exhibited yellowish-pale fur, profound listlessness, somnolence, and reduced food interest. Administration of ZJP and vitacoenzyme each provided some symptomatic relief in

their respective groups. The extent of recovery observed in the ZJPH cohort exceeded the improvements seen in the ZJPL cohort **(Figure 4c).**

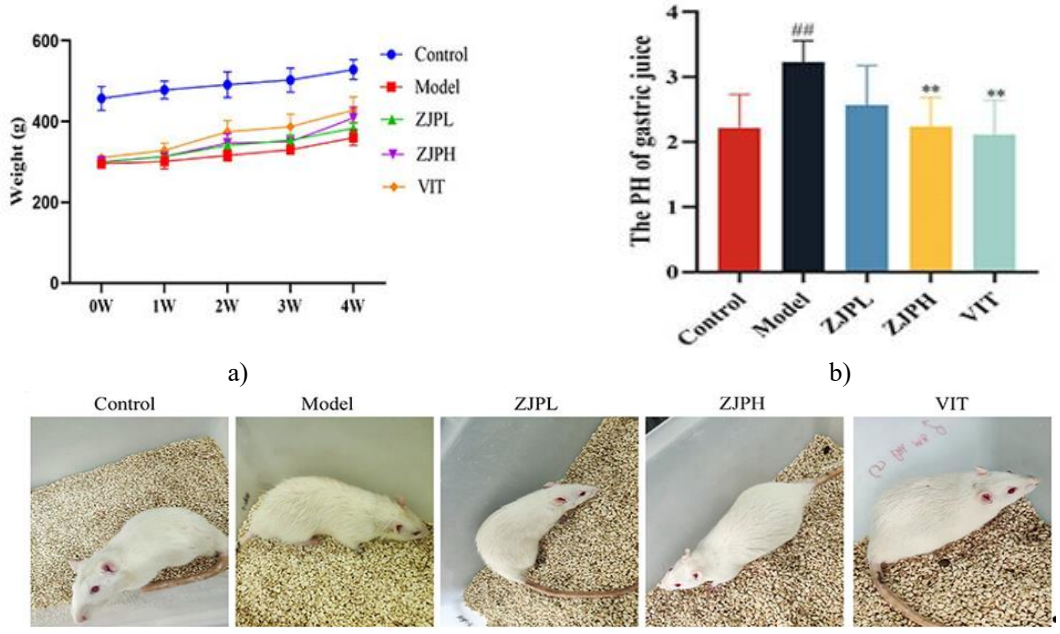

a) b)

c)

Figure 4. Effect of ZJP on general condition and body weight: (a) Changes in body weight in each group, (b) The result of the gastric juice pH test, and (c) General state of rats in the groups. All data were expressed as means ± standard deviation (SD). ANOVA analyzed multiple comparisons. ##P < 0.01 vs control group. P < 0.01 vs model group.

Abbreviations: ZJPL, Zuojin Pill low dose (1.26g/kg); ZJPH, Zuojin Pill high dose (2.52g/kg); VIT, Vitacoenzyme (200 mg/kg)..

ZJP attenuated the pathological changes of CAG rats

The gross appearance and microscopic architecture of gastric tissues were evaluated through visual inspection and histological examination, respectively. On a macroscopic level, the gastric wall of model animals appeared considerably thinner, accompanied by a shallowing of the gastric folds. Specimens from the ZJPL, ZJPH, and vitacoenzyme treatment groups, by contrast, featured deeply invaginated rugae and a richly developed mucosal layer **(Figure 5a)**.

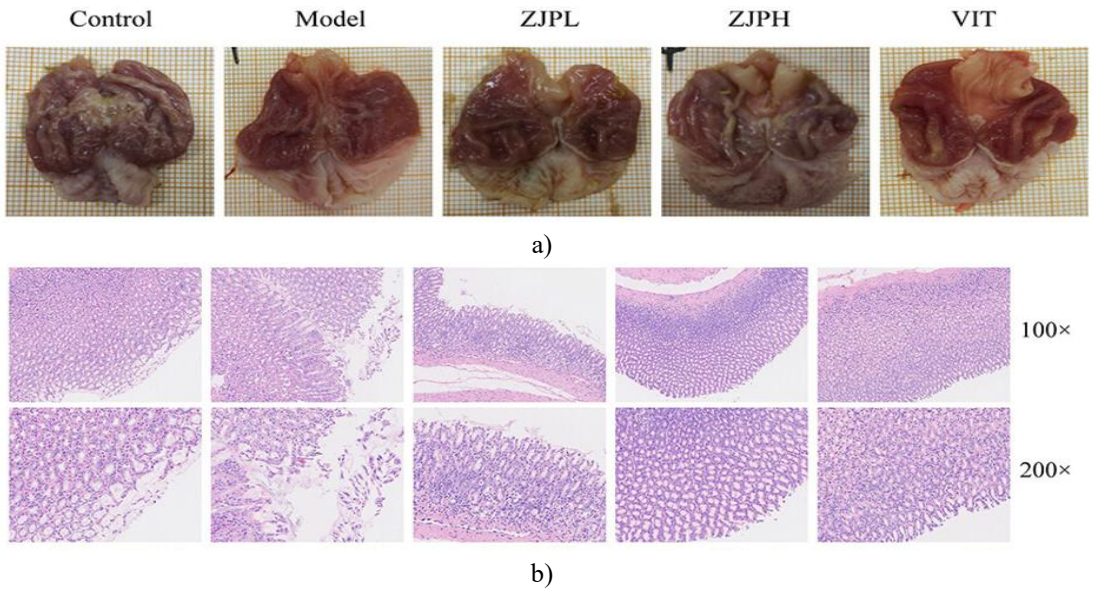

a)

b)

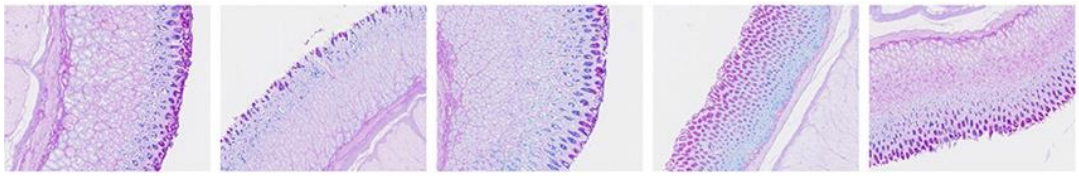

c)

Figure 5. Effect of ZJP on gastric mucosal injury: (a) Macroscopic morphology of each group, (b) HE staining of gastric histopathology, and (c) Representative images AB-PAS staining of each group. Abbreviations: ZJPL = Zuojin Pill low dose (1.26g/kg); ZJPH = Zuojin Pill high dose (2.52g/kg); VIT = Vitacoenzyme (200 mg/kg).

Microscopic tissue changes were assessed using HE-stained preparations. Sections from control animals displayed gastric mucosal lining cells and inherent glands distributed in a structured, well-organized fashion. The model rat mucosa, on the other hand, appeared shrunken and thin, with a marked scarcity of glands, haphazard cellular arrangement, and conspicuous influx of inflammatory cells. Conversely, tissue sections from the ZJPL, ZJPH, and vitacoenzyme groups demonstrated orderly cellular alignment, attenuated gland atrophy, comparatively intact glandular organization, and diminished inflammatory infiltrate **(Figure 5b)**. AB-PAS staining served to gauge the depth of the functional gastric mucosa. Compared with control values, mucosal thickness was severely reduced in the model cohort, yet supplementation with ZJP and vitacoenzyme partially restored it to varying degrees **(Figure 5c)**.

ZJP inhibited inflammatory response in CAG rats

To profile the inflammatory insult characteristic of CAG, a panel of inflammation-related mediators—TNF-α, IL-1β, IL-6, and NF-κB p65—was measured. As illustrated in **Figures 6a–6c**, circulating concentrations of TNF-α, IL-1β, and IL-6 in the model arm rose well above the values recorded for the control arm. Compared with the model condition, the ZJP-treated cohorts exhibited reductions in all three cytokines. Of note, the dampening effect achieved in the ZJPH arm was more substantial than that in the ZJPL arm. Furthermore, immunofluorescence for NF-κB p65 was performed, revealing a striking increase in its expression in the model group. ZJP therapy, however, led to a dose-dependent suppression of NF-κB p65, suggesting that ZJP's gastroprotective properties are mediated by curtailment of the inflammatory response **(Figures 6d and 6e).**

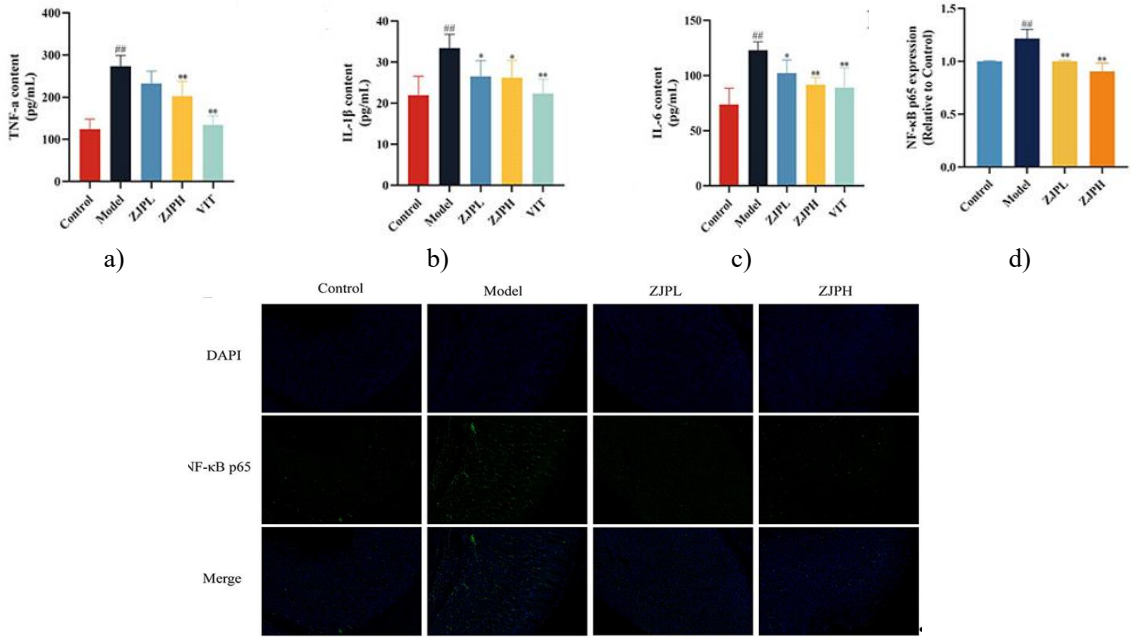

Figure 6. Effect of ZJP on inflammatory response: (a) The expression level of TNF-α in serum, (b) The expression level of IL-1β in serum, (c) The expression level of IL-6 in serum (n=6), (d) The NF-κB p65

relative expression, and (e) Representative immunofluorescence staining images in gastric mucosa showing NF-κB p65 expression (400× magnification). All data were expressed as means ± standard deviation (SD). ANOVA analyzed multiple comparisons. ##P < 0.01 vs control group. P < 0.05 and P < 0.01 vs model group. Abbreviations: ZJPL = Zuojin Pill low dose (1.26g/kg); ZJPH = Zuojin Pill high dose (2.52g/kg); VIT = Vitacoenzyme (200 mg/kg).

ZJP improved biomarkers in serum of CAG rats

To characterize the circulating profile of several well-established CAG markers, the serum content of PG I, PG II, and GAS-17 was determined. The data presented in **Figures 7a–7c** demonstrate that, relative to the control group, the model cohort experienced a dramatic drop in PG I and PG II levels, while simultaneously registering a steep increase in GAS-17 concentration. Strikingly, treatment with both ZJP and vitacoenzyme led to a significant normalization of the aforementioned indices, and the restorative effect in the ZJPH arm was more pronounced than in the ZJPL arm.

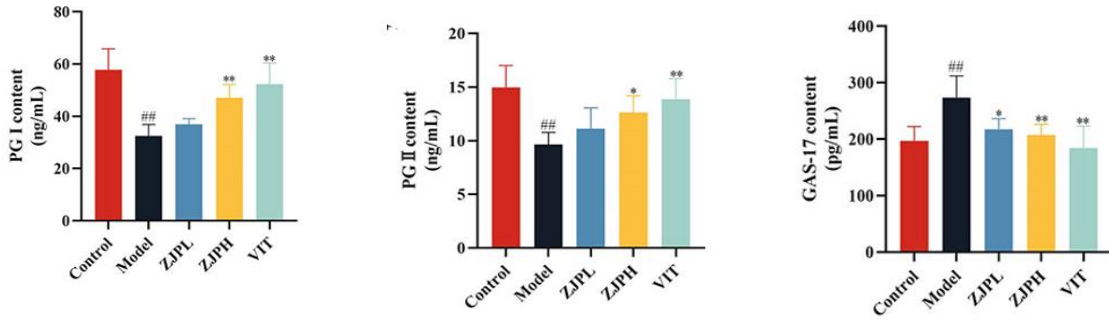

a) b) c)

Figure 7. Effect of ZJP on biomarkers in the serum of CAG: (a) The expression level of PG I in serum, (b) The expression level of PG II in serum, and (c) The expression level of GAS-17 in serum (n = 6). All data were expressed as means ± standard deviation (SD). ANOVA analyzed multiple comparisons. ##P < 0.01 vs control group. P < 0.05 and P < 0.01 vs model group. Abbreviations: ZJPL = Zuojin Pill low dose (1.26g/kg); ZJPH = Zuojin Pill high dose (2.52g/kg); VIT = Vitacoenzyme (200 mg/kg).

Network pharmacology and molecular docking predicted potential mechanism for ZJP treatment of CAG

Potential targets and cross-gene screening of ZJP and CAG

A network pharmacology-driven approach was adopted to anticipate the compositional repertoire of ZJP and disease-relevant targets for CAG, and to identify overrepresented signaling pathways, providing an analytical roadmap for subsequent mechanistic dissection. After consolidating records and eliminating redundancies, the dataset comprised 33 unique chemical constituents coupled with 826 molecule-associated targets for ZJP, plus 766 targets implicated in CAG etiology **(Figures 8a and 8b)**. As shown in **Figures 8c and 8d**, a pool of 108 intersecting genes, common to both the compound-associated and CAG-associated target collections, was retained and submitted to the STRING platform for PPI network generation. Cytoscape-based rendering of the interaction map revealed that nodes with larger diameters had higher degree scores and were identified as hub targets. These pivotal nodes exhibited functional connections with inflammatory cascades, apoptotic regulation, and mucosal barrier integrity.

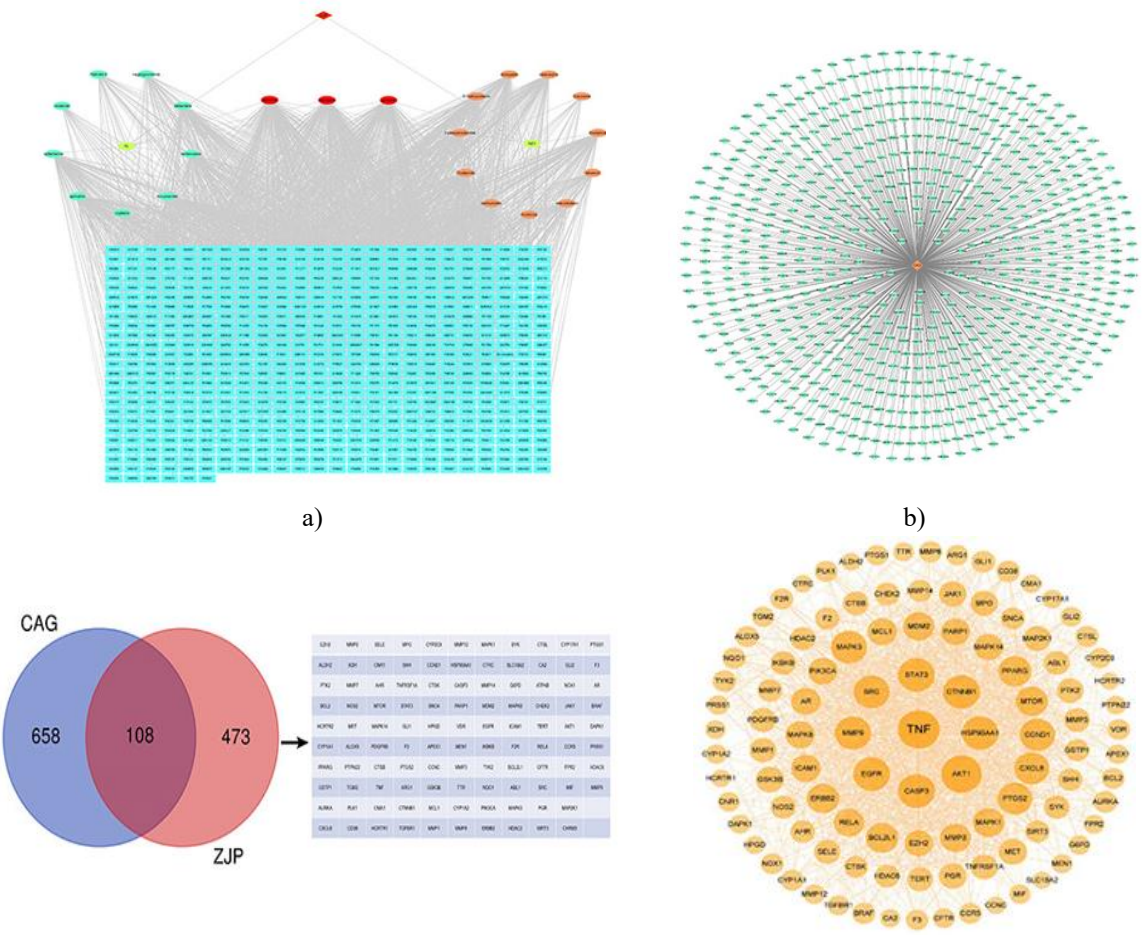

Figure 8. Network pharmacology-based prediction of ZJP treatment for CAG: (a) "ZJP- ingredients- targets" network, (b) CAG-related targets network, (c) Venn diagram, and (d) The PPI network. Abbreviations: ZJP = Zuojin Pill; HL = Coptidis Rhizoma; WZY = Euodiae Fructus.

GO and KEGG enrichment analysis and construction of PPI network

To elucidate the biological roles and principal pathways operating among the core targets in the context of CAG intervention, functional categorization via GO term and KEGG pathway overrepresentation analyses was performed. As displayed in **Figures 9a–9d**, significant enrichment was detected across the 30 foremost KEGG pathways together with the top 10 GO terms. KEGG mapping highlighted a pronounced association between the hub gene set and cascades such as the PI3K/Akt and TNF signaling pathways. Of these, the PI3K/Akt pathway was the most highly enriched. With respect to GO output, the foremost 10 biological processes connected to ZJP's anti-CAG effects were found to include negative modulation of apoptotic execution, positive modulation of RNA polymerase II-driven transcription, positive modulation of gene expression programs, signal relay, and protein phosphorylation; the principal cellular component designations covered the cytoplasmic compartment, nuclear compartment, cytosol, plasma membrane, and nucleoplasm; the leading molecular function annotations encompassed protein binding, self-association of identical proteins, ATP binding, protein kinase catalytic activity, and enzyme binding. Thereafter, a comprehensive interaction framework was assembled, weaving together the 30 top-ranked signaling pathways, the GO annotation entries harvested from enrichment analysis, and the genes populating each pathway—all of which are putatively relevant to ZJP's counteraction of CAG.

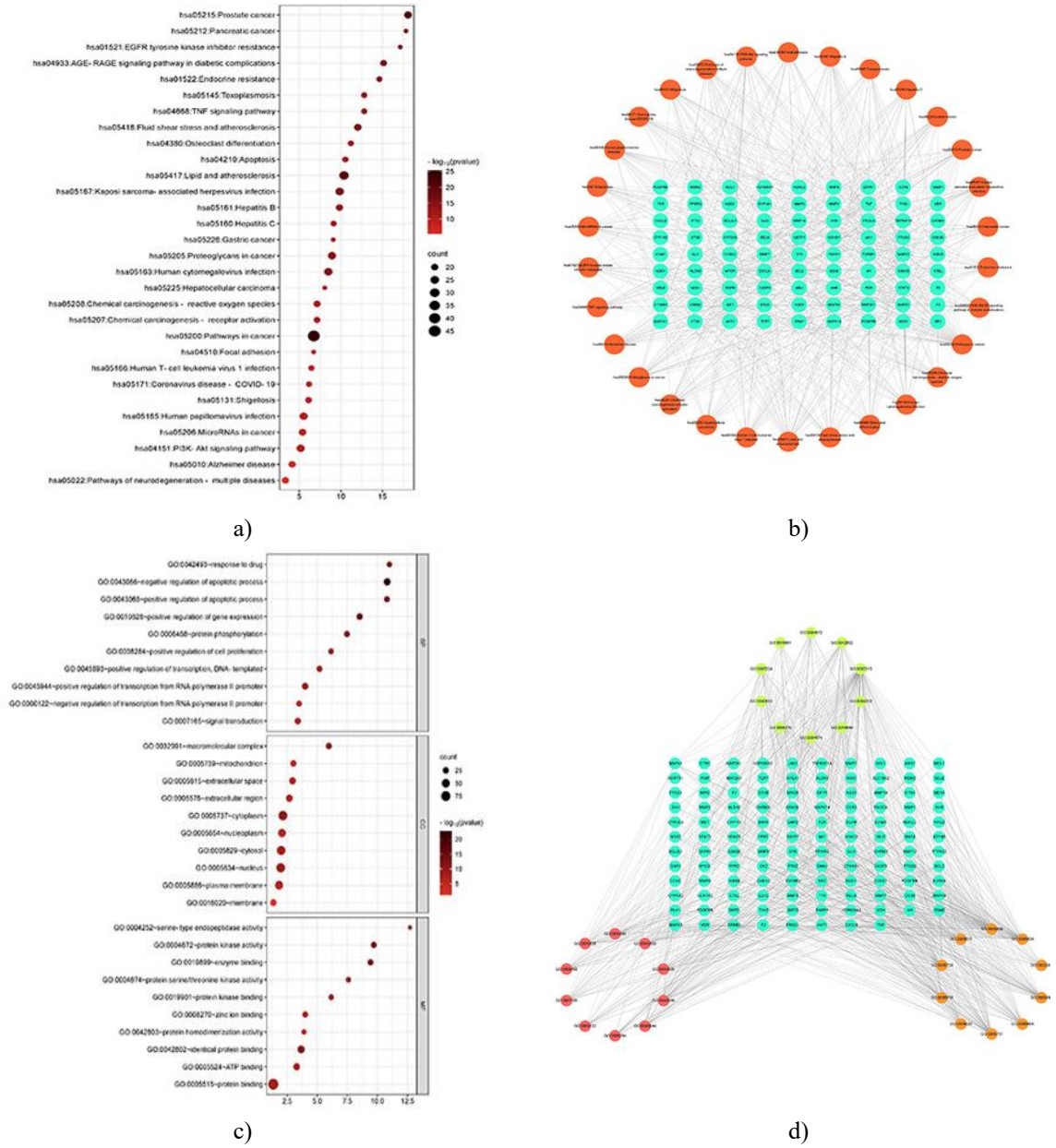

Figure 9. Enrichment analysis and gene-pathway network analysis: (a) Top 30 KEGG terms of key genes, (b) Top 10 GO terms of key genes, (c) Gene-pathway network of ZJP in CAG, and (d) Gene-GO terms network of ZJP in CAG.

ZJP regulated key genes in the treatment of CAG

In silico network pharmacology forecasts had pinpointed inflammation, apoptosis, and mucosal defense as the principal avenues through which ZJP exerts its curative action in CAG. On this basis, empirical confirmation of the corresponding targets was carried out. In contrast to the control state, the mRNA expression levels of AKT1, TNF-α, CASP3, and EGFR were substantially elevated in the model group, whereas the transcriptional level of CTNNB1 declined. Mirroring these changes, escalating doses of ZJP notably dampened the expression signals of AKT1, TNF-α, CASP3, and EGFR, while significantly potentiating CTNNB1 transcription, with the magnitude of effect following a clear dose-response relationship **(Figures 10a–10e).**

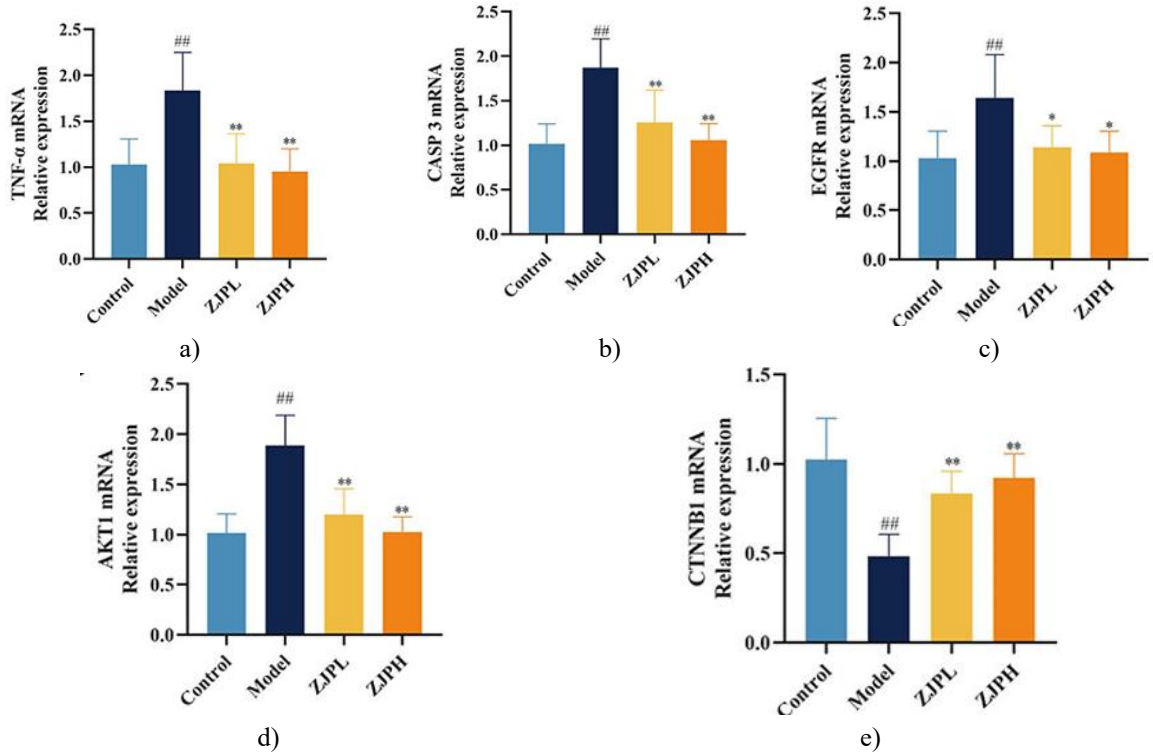

Figure 10. Effects of ZJP on key targets of CAG: (a) The TNF-α mRNA relative expression, (b) The CASP-3 mRNA relative expression, (c) The EGFR mRNA relative expression, (d) The AKT1 mRNA relative expression, and (e) The CTNNB1 mRNA relative expression (n = 6). All data were expressed as means ± standard deviation (SD). ANOVA analyzed multiple comparisons. ##P < 0.01 vs control group. P < 0.05 and P < 0.01 vs model group. Abbreviations: ZJPL = Zuojin Pill low dose (1.26g/kg); ZJPH = Zuojin Pill high dose (2.52g/kg); VIT = Vitacoenzyme (200 mg/kg).

ZJP prevented CAG by inhibiting PI3K/Akt signaling pathway

To substantiate the functional engagement of the PI3K-Akt signaling module in mediating ZJP's therapeutic influence on CAG, immunoblotting was performed to assess gastric tissue concentrations of PI3K, total Akt, and the phosphorylated species p-Akt. As shown in **Figures 11a–11c**, the model cohort demonstrated increased PI3K and p-Akt protein abundance compared with the control cohort. Compared with the model group, each drug-treated cohort showed marked suppression of PI3K and p-Akt protein levels. Levels of total Akt were not statistically different across the control, model, and ZJP-administered groups. In parallel, the p-Akt-to-Akt ratio was robustly and dose-dependently corrected following ZJP administration, compared with the untreated condition.

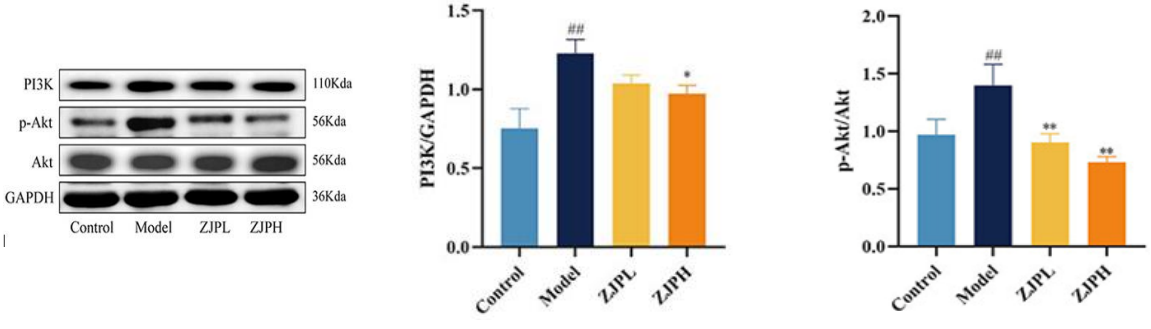

Figure 11. Effects of ZJP on PI3K/Akt signaling pathway: (a) Western blotting images of PI3K, p-Akt, and Akt, (b) The relative protein expression of PI3K, and (c) Relative protein expression of p-Akt. All data were expressed as means ± standard deviation (SD). ANOVA analyzed multiple comparisons. ##P < 0.01 vs

control group. $P < 0.05$ and $P < 0.01$ vs model group. Abbreviations: ZJPL = Zuojin Pill low dose (1.26g/kg); ZJPH = Zuojin Pill high dose (2.52g/kg); VIT = Vitacoenzyme (200 mg/kg).

ZJP inhibited apoptosis by reducing levels of apoptosis-related proteins in CAG rats

To gain deeper insight into how ZJP curbs apoptotic cell death during CAG treatment, a panel of apoptosis-associated protein markers was surveyed. As detailed in **Figures 12a–12k**, the model group relative to the control group featured steeply diminished protein signals for Bcl-2 and Bcl-xl, together with collapsed Bcl-2/Bax and Bcl-xl/Bad expression ratios, alongside prominent elevations in the protein content of Bax, Bad, Cytochrome C, cleaved-caspase-9, cleaved-caspase-3, and Apaf-1. Treatment with ZJP via oral gavage, by contrast, substantially normalized these aberrant protein patterns—including Bcl-2, Bcl-xl, Bax, Bad, cleaved-caspase-9, cleaved-caspase-3, Apaf-1, Cytochrome C, and the Bcl-2/Bax as well as Bcl-xl/Bad ratios—when juxtaposed with the model cohort, and the ZJPH arm consistently outperformed the ZJPL arm in this regard. Beyond protein-level evidence, the extent of gastric mucosal apoptosis was directly visualized by TUNEL histochemistry. Following ZJP therapy, the abundance of TUNEL-positive cells in gastric tissue sections was clearly reduced compared with the model group **(Figure 12l).**

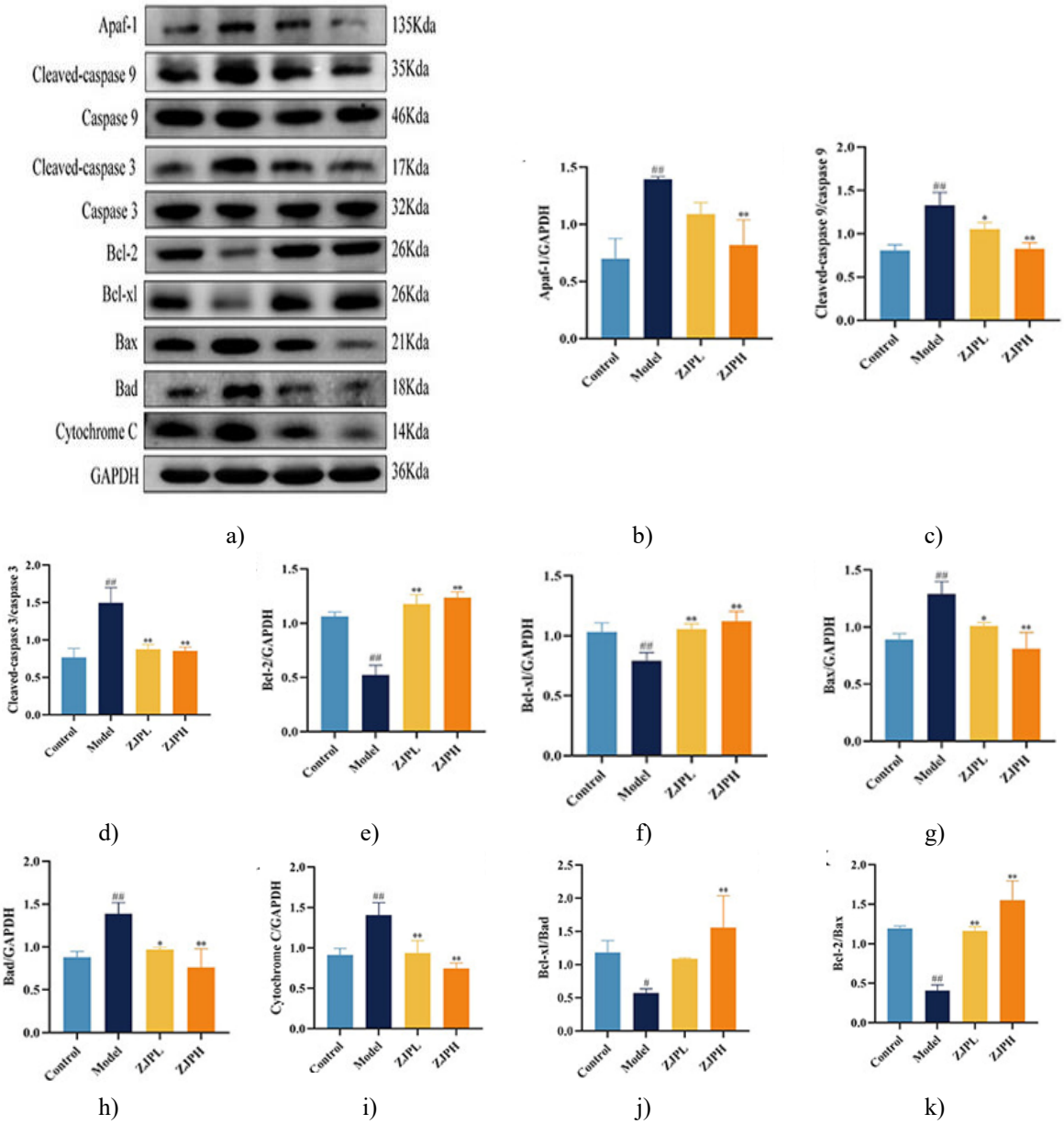

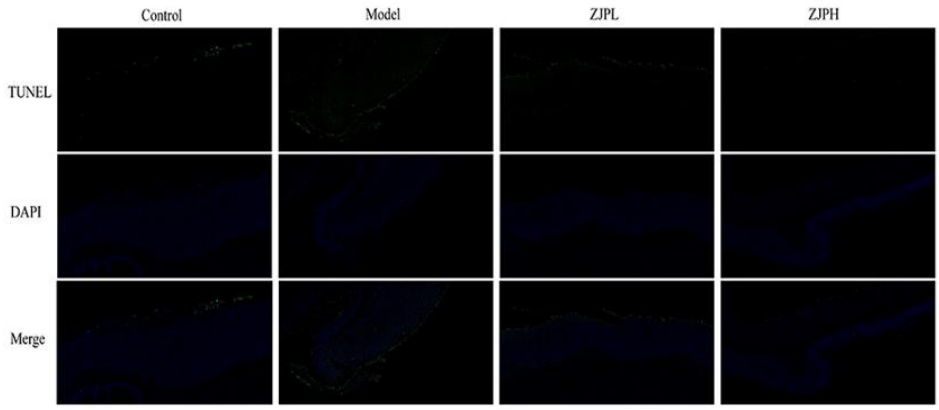

l)

Figure 12. Effects of ZJP on apoptosis-related proteins: (a) Western blotting images of apoptosis-related proteins, (b) The relative protein expression of Apaf-1, (c) The relative protein expression of cleaved-Caspase-9/ Caspase-9, (d) The relative protein expression of cleaved-caspase-3/Caspase-3, (e) The relative protein expression of Bcl-2. (f) The relative protein expression of Bcl-xl, (g) The relative protein expression of Bax, (h) The relative protein expression of Bad, (I) The relative protein expression of Cytochrome C, (j) The ratio of Bcl-xl/Bad, (k) The ratio of Bcl-2/Bax, and (l) TUNEL analysis of apoptosis in the gastric tissues of rats in each group. All data were expressed as means ± standard deviation (SD). ANOVA analyzed multiple comparisons. #P < 0.05 and ##P < 0.01 vs control group. P < 0.05 and P < 0.01 vs model group. Abbreviations: ZJPL = Zuojin Pill low dose (1.26g/kg); ZJPH = Zuojin Pill high dose (2.52g/kg); VIT = Vitacoenzyme (200 mg/kg).

ZJP PROTECTED THE INTEGRITY OF GASTRIC MUCOSA EPITHELIUM

A more complete evaluation of the gastroprotective properties exerted by ZJP on epithelial barrier integrity in CAG rats was achieved by measuring the protein expression of four tight junction and adhesion molecules: Occludin, ZO-1, Claudin-4, and E-cadherin. The analysis showed that the model group exhibited a striking reduction in protein levels of Occludin, ZO-1, Claudin-4, and E-cadherin compared with the control group. ZJP administration dramatically counteracted these deficits, restoring expression of all the above proteins, with the most pronounced restitution observed in the high-dose ZJPH group. Transcript-level quantification yielded results fully aligned with the protein data, confirming the same directional trends **(Figures 13a–13i).**

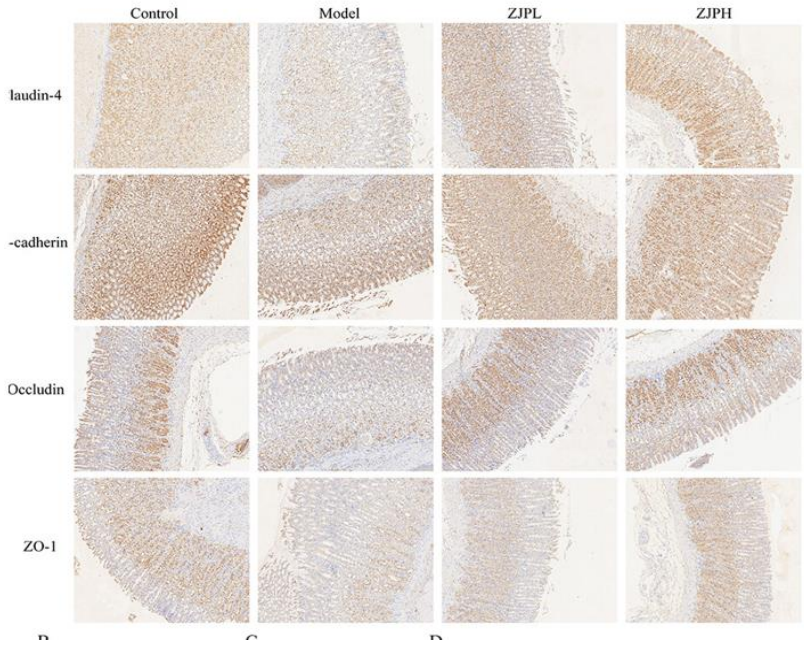

a)

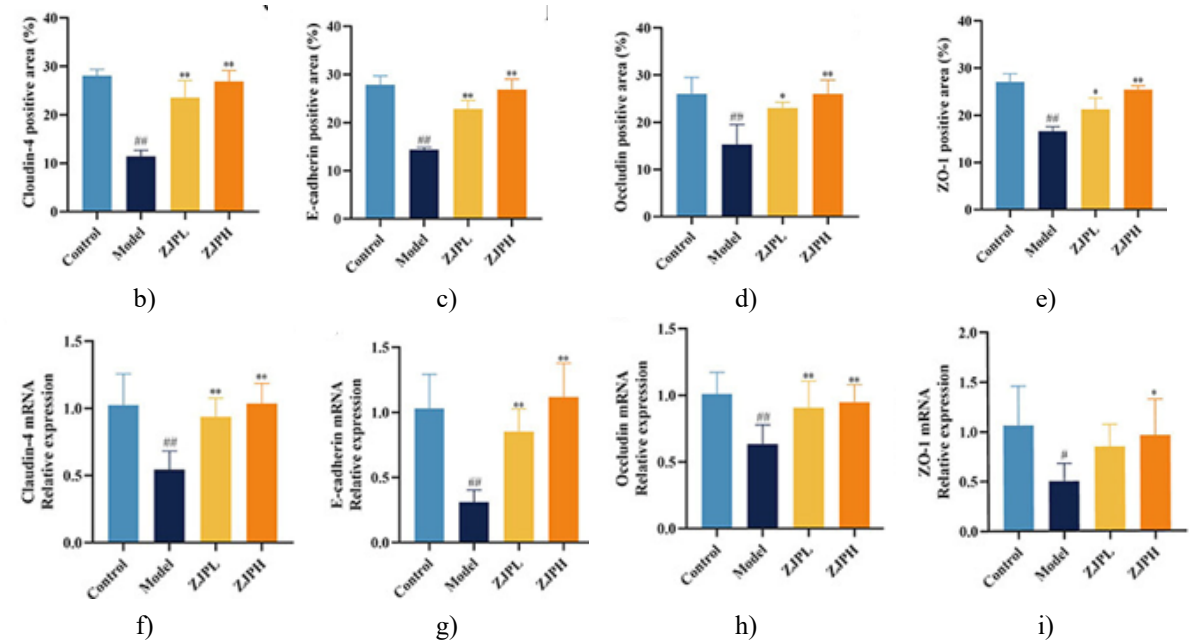

Figure 13. Effects of ZJP on mucosal integrity: (a) Images of Occludin, ZO-1, Claudin-4, and E-cadherin in rat gastric tissues were captured using immunohistochemistry (100×), (b) Claudin-4 protein expression level, (c) E-cadherin protein expression level, (d) Occludin protein expression level, (e) ZO-1 protein expression level, (f) The Claudin-4 mRNA relative expression, (g) The E-cadherin mRNA relative expression, (h) The Occludin mRNA relative expression, and (i) The ZO-1 mRNA relative expression. All data were expressed as means ± standard deviation (SD). ANOVA analyzed multiple comparisons. #P < 0.05 and ##P < 0.01 vs control group. P < 0.05 and P < 0.01 vs model group. Abbreviations: ZJPL = Zuojin Pill low dose (1.26g/kg); ZJPH = Zuojin Pill high dose (2.52g/kg); VIT = Vitacoenzyme (200 mg/kg).

Molecular docking analysis

To delve more deeply into the molecular-level mechanism by which ZJP counteracts CAG, docking simulations pairing the most critical hub targets with the most prominent active ingredients were performed. Informed by the preceding network pharmacology findings, the five top-tier targets—TNF-α, EGFR, CASP 3, AKT1, and CTNNB1—were selected, along with the three foremost bioactive constituents: quercetin (QUE), obacunone (OBA), and berberine (BBR). The corresponding PDB accession codes were assigned as follows: TNF (5UUI), EGFR (5Y9T), CASP 3 (5IBP), AKT1 (1UNQ), and CTNNB1 (1JDH). For the great majority of compound–target combinations, the computed binding free energies were more negative than −5 kcal/mol, pointing toward advantageous binding affinity and considerable complex stability between the major constituents and their protein targets **(Table 1)** [24]. The optimally ranked docking poses, rendered visually, are depicted in **Figures 14a–14c.**

Table 1. Molecular docking of key ingredients and targets.

Targets	PDB ID	Target structure	Ingredients	Binding energy (kcal/ mol)
TNF	5UUI	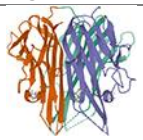	Quercetin	−5.77
			Obacunone	−6.95
			Berberine	−6.73
EGFR	5Y9T		Quercetin	−6.37
			Obacunone	−8.04
			Berberine	−7.45
CASP 3	5IBP		Quercetin	−6.29
			Obacunone	−7.15
			Berberine	−6.49
AKT1	1UNQ		Quercetin	−6.13

			Obacunone	−7.03
			Berberine	−6.47
CTNNB1	1JDH		Quercetin	−4.26
			Obacunone	−6.19
			Berberine	−5.69

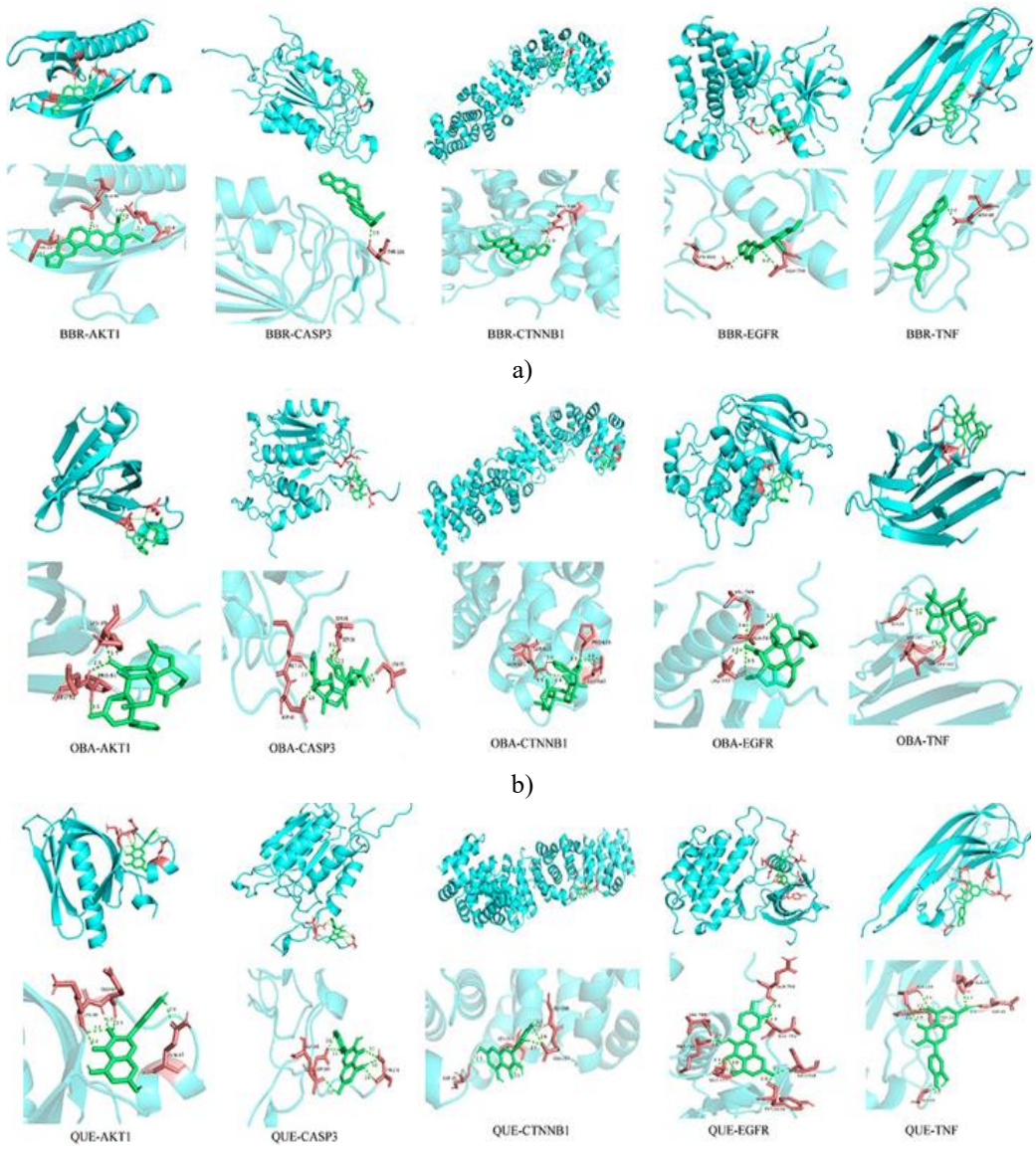

Figure 14. Docking complexes 3D diagram of 5 key targets along with 3 key ingredients: (a) 3D binding posture schematic diagram of berberine and 5 key targets, (b) 3D binding posture schematic diagram of obacunone and 5 key targets, and (c) 3D binding posture schematic diagram of quercetin and 5 key targets.

CAG is a defining precancerous stage of gastric malignancy, characterized by a high likelihood of malignant transformation. In recent times, the prevalence of CAG has surged and increasingly affects younger populations, severely undermining patient health and diminishing quality of life for an ever-larger demographic [25]. ZJP is a commonly used classical Chinese medicinal formulation that exhibits diverse pharmacological properties in the alimentary system [13]. An expanding body of research indicates that ZJP possesses inflammation-dampening, antimicrobial, and mucosa-preserving properties [12, 13, 26]. As emerging technologies advance without pause,

understanding of the mechanistic foundations underlying traditional Chinese remedies for CAG has deepened considerably. In this research effort, the prospective therapeutic mechanism of ZJP against CAG was investigated using a combined network pharmacology and confirmatory laboratory experiments approach. The body of evidence confirmed that ZJP yields a pronounced therapeutic benefit against CAG by blocking apoptotic pathways and curbing the inflammatory cascade, while repairing gastric mucosal deterioration via regulation of the PI3K/Akt signaling network, thereby offering a defined theoretical anchor for subsequent investigation of ZJP in CAG therapy **(Figure 15).**

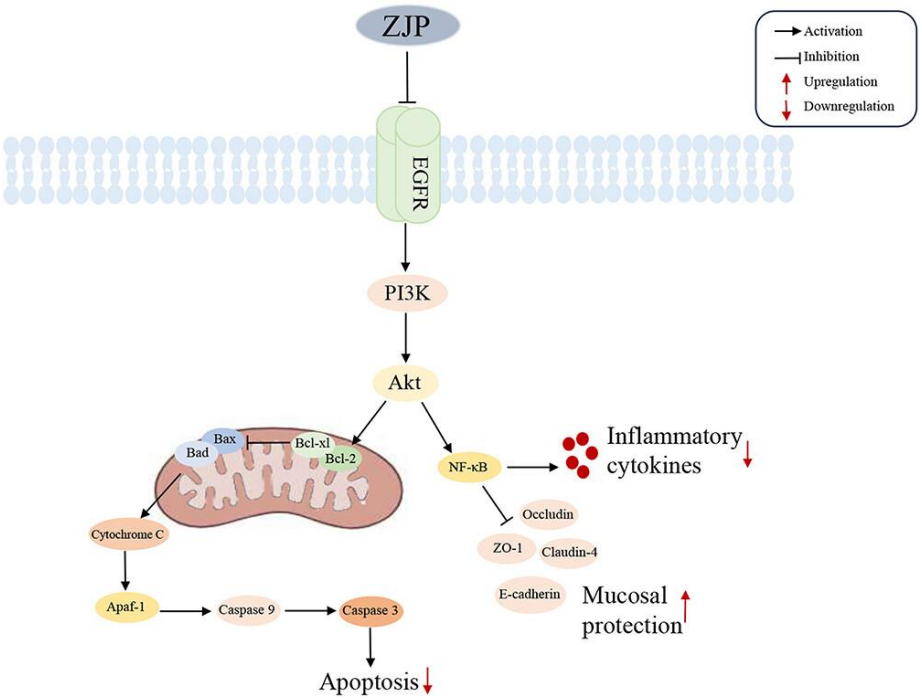

Figure 15. Potential molecular mechanism of ZJP in the treatment of CAG.

A key observation was that weight loss is a classic clinical hallmark of CAG. Throughout this study, rats allocated to the model arm experienced a significant decline in body weight, a trend that could be meaningfully reversed with ZJP. Additionally, pepsinogen (PG), an inactive precursor enzyme discharged by gastric mucosal cells, exists endogenously in two variant forms: PG I and PG II. Fluctuations in the circulating levels of PG I and PG II operate as informative surrogate markers capable of reflecting both the morphological condition and functional performance of the gastric lining [27-29]. It has been thoroughly established that depleted concentrations of PG I and PG II are characteristic of the CAG model phenotype [30]. Of equal significance, GAS-17 is a peptide hormone that participates in regulating the division, expansion, and programmed death of gastrointestinal mucosal cells, as well as gastric acid secretion. The hormone serves as a barometer of gastric mucosal functional integrity within the organism, and its circulating levels are tightly correlated with the onset and progression of gastric disorders [31, 32]. Hence, an integrated analysis of PG I, PG II, and GAS-17 readouts facilitates a more holistic and accurate diagnosis of CAG status [33]. In the present work, our data revealed that the ZJP intervention led to upregulation of PG I, PG II, and GAS-17. Accordingly, our findings lend evidentiary support to the therapeutic use of ZJP in CAG management.

Prior investigations have established that the generation of pro-inflammatory signaling molecules within the gastric epithelium potentiates inflammatory injury and that their overproduction underlies gastric mucosal pathology [34]. Numerous lines of evidence have verified that cytokine overexpression is correlated with an elevated risk of developing CAG in both animal-based experiments and human clinical settings, with several central players identified, notably TNF-α, IL-6, and IL-1β [16, 35, 36]. It warrants emphasis that TNF-α, once released, is among the most detrimental cytokines involved in CAG pathophysiology [37]. IL-1β functions as a canonical pro-inflammatory molecule that mobilizes specific immune defenses and serves as a sentinel in immune surveillance [38]. Likewise, IL-6 is a versatile pro-inflammatory cytokine produced by diverse cellular sources and plays an indispensable role in orchestrating immune homeostasis, driving inflammatory processes, and

influencing tumorigenesis [39]. NF-κB functions as a dominant redox-responsive transcriptional regulator, initiating the expression of a host of pro-inflammatory genes and modulating the synthesis of inflammatory cytokines [40]. Research has demonstrated that functional suppression of NF-κB results in diminished production of inflammatory mediators such as TNF-α, IL-6, and IL-1β [41, 42]. Our experimental outcomes indicated that ZJP potently suppressed the expression signatures of TNF-α, IL-6, IL-1β, and NF-κB p65, with more robust suppression observed in the ZJPH cohort. The constellation of results above indicates that ZJP exerts a beneficial effect on CAG by attenuating the inflammatory milieu.

Network pharmacology deciphers the biological circuitry through which pharmaceuticals exert their effects from a macroscopic or system-wide regulatory vantage point, thereby furnishing fresh investigative paradigms and technical toolkits for probing the mechanistic underpinnings of TCM and its composite formulations [43]. In this study, a network pharmacology-based strategy was used to identify the bioactive constituents, their cognate targets, and the pharmacological pathways through which ZJP operates in the management of CAG. Among the pathways identified, the PI3K/Akt signaling cascade emerged as a critical conduit implicated in CAG therapy, delivering curative benefits by suppressing inflammation, blocking apoptosis, and preserving the gastric mucosal lining. Beyond regulating cellular apoptosis, migration, differentiation, and metabolic processes, the PI3K/Akt axis also participates in gastric mucosal epithelial regeneration and facilitates the initiation and progression of gastric neoplasms [44]. Prior reports have documented that the epidermal growth factor receptor (EGFR) can trigger the PI3K signaling cascade [45, 46]. Akt constitutes a serine/threonine-directed protein kinase positioned downstream of PI3K within the intracellular signal relay apparatus. Phosphorylation of Akt unleashes its catalytic function, culminating in the phosphorylation of downstream effectors and consequent modulation of both programmed cell death and inflammatory signaling [47-49]. In our experimental context, ZJP ameliorated CAG by engaging the PI3K/Akt pathway, chiefly by markedly reducing the p-Akt/Akt ratio and decreasing PI3K abundance.

It has been widely acknowledged that mitochondria serve as command hubs governing bioenergetics, metabolism, and apoptotic execution, with their functions tightly orchestrated by a diverse array of intrinsic and extrinsic cues, including chemical signals and members of the Bcl-2 and caspase families [50]. In general, the mitochondrial apoptosis pathway is tightly regulated by the Bcl-2 family, which includes guardians of cell survival (Bcl-2 and Bcl-xl) and promoters of cell death (Bax and Bad) [51]. The equilibrium between these opposing factions directly dictates mitochondrial physiological competence [52, 53]. It has been firmly established that activated Akt can phosphorylate Bad at Ser136, thereby attenuating its interaction with Bcl-xl and Bcl-2 and, consequently, exerting an anti-apoptotic influence [54]. Moreover, pro-apoptotic proteins trigger cell death by breaching mitochondrial membrane integrity, leading to a collapse of the mitochondrial membrane potential and biochemical disturbances between the inner and outer mitochondrial compartments. These events ultimately force the release of cytochrome c from the mitochondrial interior into the cytoplasm. In turn, Apaf-1 becomes activated and assembles into an apoptosome platform, which subsequently engages and activates caspase-3, setting the apoptotic machinery in motion [55, 56]. Caspases represent a distinct class of proteolytic enzymes, also known as aspartate-specific cysteine proteases, that play pivotal roles in orchestrating apoptotic signaling cascades. Caspase-9 acts as the initiator caspase within the mitochondrial pathway; it is recruited and activated by the apoptosome complex and, in turn, proteolytically activates the downstream executioner caspase-3, driving the cell toward its ultimate demise [51, 57]. Within the scope of this investigation, we observed that ZJP sharply reduced the cytosolic pool of Cytochrome c, along with the protein expression levels of Bax, Bad, cleaved-caspase-9, cleaved-caspase-3, and Apaf-1, while concurrently and significantly elevating the protein signals of Bcl-2, Bcl-xl, the mitochondrial retention of Cytochrome c, and the expression ratios of Bcl-2/Bax and Bcl-xl/Bad. Collectively, these observations indicate that the therapeutic efficacy of ZJP in CAG is closely linked to its ability to prevent apoptotic cell death.

The gastric mucosal barrier is a vital defensive apparatus that protects the organism from pathogenic invasion and maintains gastric homeostasis. Once its integrity is breached, the onset and advancement of gastric pathologies can ensue [58, 59]. Among the principal architectural elements of this barrier are cell junctions, with tight junctions representing the most critical membrane protein assemblies within these structures, composed of occludin, claudins, ZOs, and junction adhesion molecule (JAM) [60]. It is widely recognized that ZO-1 functions as a scaffolding protein of the tight junction and is routinely used as a metric for assessing barrier competence and permeability status [61]. Furthermore, occludin is an integral transmembrane protein residing at tight junctions, and boosting its abundance would strengthen intercellular adhesion [62]. Of note, evidence suggests that claudin-

4 can concentrate occludin and engage in interplay with ZO-1; moreover, the expression profile of claudin-4 bears a close relationship to gastric malignancy [63].

Additionally, earlier reports have shown that E-cadherin mediates cell-to-cell adhesion and maintains tissue structural cohesion [64]. Within our investigation, the expression levels of ZO-1, E-cadherin, and occludin were markedly depressed, whereas claudin-4 expression was conspicuously elevated in the model cohort, implying that CAG disrupted the mucosal lining and heightened the permeability of the gastric epithelium. Notably, ZJP administration restored the expression of ZO-1, E-cadherin, claudin-4, and occludin, indicating that ZJP can strengthen the gastric mucosal defense barrier.

Although the present study delineated the therapeutic benefit of ZJP against CAG through an integrative biological approach and elucidated the molecular mechanisms by which ZJP ameliorates CAG via the PI3K/Akt signaling pathway, certain limitations persist. For instance, the contribution of individual constituents within ZJP to its anti-CAG effects has yet to be experimentally validated. Moreover, while this investigation revealed that ZJP suppresses apoptosis and attenuates inflammation and gastric mucosal barrier damage through the PI3K/Akt signaling axis, no reciprocal validation employing inhibitors or activators targeting the PI3K/Akt pathway was performed within the experimental framework. Consequently, future efforts will be directed toward further enriching and refining this line of inquiry, with the aim of comprehensively and systematically unraveling the molecular mechanisms and material foundation underlying ZJP's action in CAG, thereby establishing a research cornerstone for the rational clinical deployment of ZJP.

Conclusion

In summary, our findings substantiate that ZJP exerts a curative effect on CAG by modulating the gastric mucosal barrier, dampening inflammatory responses, and inhibiting apoptotic processes through the PI3K/Akt signaling cascade. This investigation provides both a methodological and a theoretical platform for further elucidating the pharmacological mechanism of action of ZJP in the management of CAG.

Acknowledgments: This research was financially supported by the Major Program of the National Natural Science Foundation of China (No. 82192915), the National Key Research and Development Program (No. 2018YFC1704500), and the China Postdoctoral Science Foundation (No. 2023M730115).

Conflict of Interest: None

Financial Support: None

Ethics Statement: All animal experiments were conducted in accordance with the Laboratory Care and Use Guidelines. The research was approved by the Ethics Committee of the Chinese PLA General Hospital (Approval ID: IACUC-2021-0022).

References

1. Jayavelu ND, Bar NS. Metabolomic studies of human gastric cancer: review. World J Gastroenterol. 2014;20(25):8092-101.
2. Vannella L, Lahner E, Annibale B. Risk for gastric neoplasias in patients with chronic atrophic gastritis: a critical reappraisal. World J Gastroenterol. 2012;18(12):1279-85.
3. Bray F, Ferlay J, Soerjomataram I, Siegel RL, Torre LA, Jemal A. Global cancer statistics 2018: GLOBOCAN estimates of incidence and mortality worldwide for 36 cancers in 185 countries. CA Cancer J Clin. 2018;68(6):394-424.
4. Zhenyukh O, Civantos E, Ruiz-Ortega M, Sánchez MS, Vázquez C, Peiró C, et al. High concentration of branched-chain amino acids promotes oxidative stress, inflammation and migration of human peripheral blood mononuclear cells via mTORC1 activation. Free Radic Biol Med. 2017;104:165-77.
5. Han L, Li T, Wang Y, Zhang M, Zhao Y, Liu X, et al. Weierning, a Chinese patent medicine, improves chronic atrophic gastritis with intestinal metaplasia. J Ethnopharmacol. 2023;309:116345.

6. Li Z, Wu C, Li L, Wang X, Liu B, Huang Q, et al. Effect of long-term proton pump inhibitor administration on gastric mucosal atrophy: a meta-analysis. Saudi J Gastroenterol. 2017;23(4):222-8.
7. Donzelli A. Helicobacter pylori eradication? Gastroenterology. 2016;151(4):773-4.
8. Nazari M, Taghizadeh A, Orafaei H, Boghratian A, Ghannadi A, Rashidi M, et al. Nausea and vomiting in Iranian traditional medicine based on Avicenna's viewpoint. Electron Physician. 2015;7(2):1047-53.
9. Hamidpour R, Hamidpour M, Hamidpour S, Shahlari M, Sohraby M, Shahlari N, et al. Cinnamon from the selection of traditional applications to its novel effects on the inhibition of angiogenesis in cancer cells and prevention of Alzheimer's disease, and a series of functions such as antioxidant, anticholesterol, antidiabetes, antibacterial, antifungal, nematicidal, acaracidal, and repellent activities. J Tradit Complement Med. 2015;5(2):66-70.
10. Liang F, Cooper EL, Wang H, Zhang J, Guo J, Li Y, et al. Acupuncture and immunity. Evid Based Complement Alternat Med. 2015;2015:260620.
11. El Khoury D, Cuda C, Luhovyy BL, Anderson GH. Beta glucan: health benefits in obesity and metabolic syndrome. J Nutr Metab. 2012;2012:851362.
12. Wei Y, Wang R, Ren S, Ma X, Xie S, Tong Y, et al. Zuojin pill ameliorates inflammation in indomethacin-induced gastric injury via inhibition of MAPK pathway. J Ethnopharmacol. 2021;275:114103.
13. Wen J, Wu S, Ma X, Wang R, Tong Y, Xie S, et al. Zuojin pill attenuates Helicobacter pylori-induced chronic atrophic gastritis in rats and improves gastric epithelial cell function in GES-1 cells. J Ethnopharmacol. 2022;285:114855.
14. Peng QX, Cai HB, Peng JL, Zhou QM, Chen JH, Zheng YL, et al. Extract of Zuojin Pill induces apoptosis of SGC-7901 cells via mitochondria-dependent pathway. Chin J Integr Med. 2015;21(11):837-45.
15. Wang QS, Zhu XN, Jiang HL, Wang GF, Cui YL, Ye WC, et al. Protective effects of alginate-chitosan microspheres loaded with alkaloids from Coptis chinensis Franch. and Evodia rutaecarpa (Juss.) Benth. (Zuojin Pill) against ethanol-induced acute gastric mucosal injury in rats. Drug Des Devel Ther. 2015;9:6151-65.
16. Ma X, Xie S, Wang R, Tong Y, Wei Y, Wen J, et al. Metabolomics profiles associated with the treatment of Zuojin Pill on patients with chronic nonatrophic gastritis. Front Pharmacol. 2022;13:898680.
17. Li S, Zhang B. Traditional Chinese medicine network pharmacology: theory, methodology and application. Chin J Nat Med. 2013;11(2):110-20.
18. Li Q, Lan T, He S, Zhao X, Zhang M, Wu Y, et al. A network pharmacology-based approach to explore the active ingredients and molecular mechanism of Lei-Gong-Gen formula granule on a spontaneously hypertensive rat model. Chin Med (Lond). 2021;16(1):99.
19. Xiang SY, Zhao J, Lu Y, Wang M, Chen X, Li Y, et al. Network pharmacology-based identification for therapeutic mechanism of Ling-Gui-Zhu-Gan decoction in the metabolic syndrome induced by antipsychotic drugs. Comput Biol Med. 2019;110:1-7.
20. Guo W, Huang J, Wang N, Tan HY, Cheung F, Chen F, et al. Integrating network pharmacology and pharmacological evaluation for deciphering the action mechanism of herbal formula Zuojin Pill in suppressing hepatocellular carcinoma. Front Pharmacol. 2019;10:1185.
21. Cui J, Liu Y, Hu Y, Wang C, Zhang L, Li X, et al. NMR-based metabonomics and correlation analysis reveal potential biomarkers associated with chronic atrophic gastritis. J Pharm Biomed Anal. 2017;132:77-86.
22. Tong Y, Wang R, Liu X, Ma X, Xie S, Wei Y, et al. Zuojin Pill ameliorates chronic atrophic gastritis induced by MNNG through the TGF-β1/PI3K/Akt axis. J Ethnopharmacol. 2021;271:113893.
23. Kangwan N, Pintha K, Lekawanvijit S, Suttajit M, Rosmarin D, Kukongviriyapan V, et al. Rosmarinic acid enriched fraction from Perilla frutescens leaves strongly protects indomethacin-induced gastric ulcer in rats. Biomed Res Int. 2019;2019:9514703.
24. Hu Y, Liu T, Zheng G, Xin Y, Qin J, Sun D, et al. Mechanism exploration of 6-gingerol in the treatment of atherosclerosis based on network pharmacology, molecular docking and experimental validation. Phytomedicine. 2023;115:154835.
25. Sun Y, Wang S, Qi M, Zhang X, Zhao L, Chen Y, et al. Psychological distress in patients with chronic atrophic gastritis: the risk factors, protection factors, and cumulative effect. Psychol Health Med. 2018;23(7):797-803.
26. Wang J, Zhang T, Zhu L, Wang S, Huang J, Liu Y, et al. Anti-ulcerogenic effect of Zuojin Pill against ethanol-induced acute gastric lesion in animal models. J Ethnopharmacol. 2015;173:459-67.

27. Guo K, Li Z, Qiu B, Wang Y, Zhang J, Liu H, et al. Analysis of gastric diseases and their symptoms based on indexes of pepsinogen I (PGI) and pepsinogen II (PGII): take 1106 patients as samples. Cell Microbiol. 2022;2022:1-6.
28. Cuomo P, Papaianni M, Capparelli R, Colonna G, Iannaccone M, Iannelli D, et al. The role of formyl peptide receptors in permanent and low-grade inflammation: Helicobacter pylori infection as a model. Int J Mol Sci. 2021;22(7):3706.
29. Booth AL, Gonzalez RS. Helicobacter pylori colonisation of duodenal foveolar metaplasia requires concurrent gastric infection. J Clin Pathol. 2021;74(8):537-9.
30. Chen X, Zhang J, Wang R, Liu X, Ma X, Tong Y, et al. UPLC-Q-TOF/MS-based serum and urine metabonomics study on the ameliorative effects of palmatine on Helicobacter pylori-induced chronic atrophic gastritis. Front Pharmacol. 2020;11:586954.
31. Koivurova OP, Koskela R, Blomster T, Sipponen P, Karttunen TJ, Puolakkainen P, et al. Serological biomarker panel in diagnosis of atrophic gastritis and Helicobacter pylori infection in gastroscopy referral patients: clinical validation of the new-generation GastroPanel® test. Anticancer Res. 2021;41(11):5527-37.
32. Kim YJ, Chung WC, Kim DB. Efficacy of bismuth added to standard triple therapy as the first-line eradication regimen for Helicobacter pylori infection. Helicobacter. 2021;26(3):e12792.
33. Zagari RM, Rabitti S, Greenwood DC, Eusebi LH, Vestito A, Bazzoli F, et al. Systematic review with meta-analysis: diagnostic performance of the combination of pepsinogen, gastrin-17 and anti-Helicobacter pylori antibodies serum assays for the diagnosis of atrophic gastritis. Aliment Pharmacol Ther. 2017;46(7):657-67.
34. Antonisamy P, Arasu MV, Dhanasekaran M, Choi KC, Aravinthan A, Kim NS, et al. Protective effects of trigonelline against indomethacin-induced gastric ulcer in rats and potential underlying mechanisms. Food Funct. 2016;7(1):398-408.
35. Tong Y, Zhao X, Wang R, Ma X, Xie S, Wei Y, et al. Therapeutic effect of berberine on chronic atrophic gastritis based on plasma and urine metabolisms. Eur J Pharmacol. 2021;908:174335.
36. Wang B, Zhou W, Zhang H, Li Y, Chen X, Zhao J, et al. Exploring the effect of Weifuchun capsule on the toll-like receptor pathway mediated HES6 and immune regulation against chronic atrophic gastritis. J Ethnopharmacol. 2023;303:115930.
37. Tong Y, Liu L, Wang R, Ma X, Xie S, Wei Y, et al. Berberine attenuates chronic atrophic gastritis induced by MNNG and its potential mechanism. Front Pharmacol. 2021;12:644638.
38. Beales IL, Calam J. Interleukin 1 beta and tumour necrosis factor alpha inhibit acid secretion in cultured rabbit parietal cells by multiple pathways. Gut. 1998;42(2):227-34.
39. Unver N, McAllister F. IL-6 family cytokines: key inflammatory mediators as biomarkers and potential therapeutic targets. Cytokine Growth Factor Rev. 2018;41:10-7.
40. Tang X, Chen X, Li X, Wang Y, Zhang H, Liu J, et al. The TLR4-mediated inflammatory signal pathway might be involved in drug resistance in drug-resistant epileptic rats. J Neuroimmunol. 2022;365:577802.
41. Li H, Tang D, Qi C, Liu P, Wang S, Li S, et al. Forsythiaside inhibits bacterial adhesion on titanium alloy and attenuates Ti-induced activation of nuclear factor-κB signaling-mediated macrophage inflammation. J Orthop Surg Res. 2018;13(1):139.
42. Zhou X, Zhang L, Lie L, Xiao Y, Li W, Peng X, et al. MxA suppresses TAK1-IKKα/β-NF-κB mediated inflammatory cytokine production to facilitate Mycobacterium tuberculosis infection. J Infect. 2020;81(2):231-41.
43. Jing C, Sun Z, Xie X, Wang J, Liu X, Zhang Y, et al. Network pharmacology-based identification of the key mechanism of Qinghuo Rougan Formula acting on uveitis. Biomed Pharmacother. 2019;120:109381.
44. Qiu W, Leibowitz B, Zhang L, Yu J, Zhang Y, Lu P, et al. Growth factors protect intestinal stem cells from radiation-induced apoptosis by suppressing PUMA through the PI3K/AKT/p53 axis. Oncogene. 2010;29(11):1622-32.
45. Tiemin P, Fanzheng M, Peng X, Jihua H, Ruipeng S, Yaliang H, et al. MUC13 promotes intrahepatic cholangiocarcinoma progression via EGFR/PI3K/AKT pathways. J Hepatol. 2020;72(4):761-73.
46. Kim SH, Kim JY, Park SY, Bae SH, Hong SP, Cho KA, et al. Activation of the EGFR-PI3K-CaM pathway by PRL-1-overexpressing placenta-derived mesenchymal stem cells ameliorates liver cirrhosis via ER stress-dependent calcium. Stem Cell Res Ther. 2021;12(1):551.
47. Jiang R, Tang J, Zhang X, Wang Y, Shi Y, Liu Z, et al. CCN1 promotes inflammation by inducing IL-6 production via α6β1/PI3K/Akt/NF-κB pathway in autoimmune hepatitis. Front Immunol. 2022;13:810671.

48. Miao Z, Miao Z, Wang S, Liu Y, Zhang X, Li H, et al. Quercetin antagonizes imidacloprid-induced mitochondrial apoptosis through PTEN/PI3K/AKT in grass carp hepatocytes. Environ Pollut. 2021;290:118036.
49. Pappalardo F, Russo G, Candido S, Pennisi M, Cavalieri S, Motta S, et al. Computational modeling of PI3K/AKT and MAPK signaling pathways in melanoma cancer. PLoS One. 2016;11(3):e0152104.
50. Tsai HF, Hsu PN. Modulation of tumor necrosis factor-related apoptosis-inducing ligand (TRAIL)-mediated apoptosis by Helicobacter pylori in immune pathogenesis of gastric mucosal damage. J Microbiol Immunol Infect. 2017;50(1):4-9.
51. He H, Feng M, Xu H, Wang H, Zhang Y, Wang J, et al. Total triterpenoids from the fruits of Chaenomeles speciosa exerted gastroprotective activities on indomethacin-induced gastric damage via modulating microRNA-423-5p-mediated TFF/NAG-1 and apoptotic pathways. Food Funct. 2020;11(1):662-79.
52. Han B, Jiang P, Li Z, Yu Y, Huang T, Ye X, et al. Coptisine-induced apoptosis in human colon cancer cells (HCT-116) is mediated by PI3K/Akt and mitochondrial-associated apoptotic pathway. Phytomedicine. 2018;48:152-60.
53. Wang J, Hu S, Wang J, Liu Y, Zhang Y, Yang X, et al. Fucoidan from Acaudina molpadioides protects pancreatic islet against cell apoptosis via inhibition of inflammation in type 2 diabetic mice. Food Sci Biotechnol. 2016;25(1):293-300.
54. Wang L, Liu X, Kang Q, Zhang Y, Zhao Y, Li H, et al. Nrf2 overexpression decreases vincristine chemotherapy sensitivity through the PI3K-AKT pathway in adult B-cell acute lymphoblastic leukemia. Front Oncol. 2022;12:876556.
55. Wang J, Wang A, He H, Feng M, Zhang Y, Xu H, et al. Trametenolic acid B protects against cerebral ischemia and reperfusion injury through modulation of microRNA-10a and PI3K/Akt/mTOR signaling pathways. Biomed Pharmacother. 2019;112:108692.
56. Zhang Y, Xu H, He H, Wang J, Feng M, Liu Y, et al. Total triterpenes from the fruits of Chaenomeles speciosa (Sweet) Nakai protects against indomethacin-induced gastric mucosal injury: involvement of TFF1-mediated EGF/EGFR and apoptotic pathways. J Pharm Pharmacol. 2020;72(3):409-23.
57. Kim B, Srivastava SK, Kim SH. Caspase-9 as a therapeutic target for treating cancer. Expert Opin Ther Targets. 2015;19(1):113-27.
58. Meyer AR, Goldenring JR. Injury, repair, inflammation and metaplasia in the stomach. J Physiol. 2018;596(17):3861-7.
59. Ye HY, Shang ZZ, Zhang FY, Wang YX, Liu J, Chen L, et al. Dendrobium huoshanense stem polysaccharide ameliorates alcohol-induced gastric ulcer in rats through Nrf2-mediated strengthening of gastric mucosal barrier. Int J Biol Macromol. 2023;236:124001.
60. Schulzke JD, Fromm M. Tight junctions: molecular structure meets function. Ann N Y Acad Sci. 2009;1165:1-6.
61. Gao A, Xia T, Peng Z, Wang H, Li J, Zhang Y, et al. The ethanolic extract of peanut shell attenuates the depressive-like behaviors of mice through modulation of inflammation and gut microbiota. Food Res Int. 2023;168:112765.
62. Ren L, Feng W, Shao J, Zhang Y, Wang H, Liu X, et al. Diethyldithiocarbamate-copper nanocomplex reinforces disulfiram chemotherapeutic efficacy through light-triggered nuclear targeting. Theranostics. 2020;10(14):6384-98.
63. Müller SL, Portwich M, Schmidt A, Utepbergenov DI, Huber O, Blasig IE, et al. The tight junction protein occludin and the adherens junction protein alpha-catenin share a common interaction mechanism with ZO-1. J Biol Chem. 2005;280(5):3747-56.
64. Derk J, Como C, Jones H, Liu Y, Schwaberow N, Iacovino M, et al. Formation and function of the meningeal arachnoid barrier around the developing mouse brain. Dev Cell. 2023;58(8):635-44.e4.